The plasma-wall transition with collisions and an oblique magnetic field: Reversal of potential drops at grazing incidences

J. Moritz (iD), M. Lesur (iD), E. Faudot, S. Devaux (iD), S. Heuraux (iD), and J. Ledig

View Online   Export Citation   CrossMark

The plasma-wall transition with collisions and an oblique magnetic field: Reversal of potential drops at grazing incidences

J. Moritz,[a] M. Lesur, E. Faudot, S. Devaux, S. Heuraux, and J. Ledig

AFFILIATIONS

Institut Jean Lamour, UMR 7198 CNRS—Université de Lorraine, Campus Artem, 2 allée André Guinier, 54011 Nancy, France

[a] jerome.moritz@univ-lorraine.fr

ABSTRACT

The plasma-wall transition is studied by using 1d3V particle-in-cell simulations in the case of a one dimensional plasma bounded by two absorbing walls separated by 200 Debye lengths (λ_d). A constant and oblique magnetic field is applied to the system, with an amplitude such that $r < \lambda_d < R$, where r and R are the electron and ion Larmor radii, respectively. Collisions with neutrals are taken into account and modelled by an energy conservative operator, which randomly reorients ion and electron velocities. The plasma-wall transition (PWT) is shown to depend on both the angle of incidence of the magnetic field with respect to the wall, θ, and on the ion mean-free-path to Larmor radius ratio, λ_{ci}/R. In the very low collisionality regime ($\lambda_{ci} \gg R$) and for a large angle of incidence, the PWT consists of the classical tri-layer structure (Debye sheath/Chodura sheath/pre-sheath) from the wall towards the center of the plasma. The drops of potential within different regions are well consistent with already published models. However, when $\sin\theta \leq R/\lambda_{ci}$ or with the ordering $\lambda_{ci} < R$, collisions cannot be neglected, leading to the disappearance of the Chodura sheath. In this case, a collisional model yields analytic expressions for the potential drop in the quasi-neutral region and explains, in qualitative and quantitative agreement with the simulation results, its reversal below a critical angle derived in this paper, a regime possibly met in the scrape-off layers of tokamaks. It is further shown that the potential drop in the Debye sheath slightly varies with the collisionality for $\lambda_{ci} \gg R$. However, it tends to decrease with λ_{ci} in the high collisionality regime, until the Debye sheath finally vanishes.

Published under license by AIP Publishing. https://doi.org/10.1063/1.5061832

I. INTRODUCTION

Sheaths are space-charged regions that take place at plasma boundaries in order to balance ion and electron losses. The material surface in contact with the plasma can be an electrode or the wall of any reactor. It becomes negatively charged due to the high velocity of electrons with respect to their positive counterpart. An electric field is built up at the vicinity of the negatively charged wall and then repels electrons and attracts ions, giving rise to the non-neutral regions called "sheaths."

Sheath formation is of paramount importance for many applications in plasma physics, such as Langmuir probe measurements in low temperature plasma, fabrication processes of nano-materials, objects, or thin films,[1] reactors in fusion plasma, where the plasma-wall transition (PWT) can lead to prejudicial heating and erosion of the surface coating,[2] and spacecrafts,

where onboard instruments can be affected by surface charging.[3] Sheaths have then been studied theoretically for several decades for the purpose of better understanding and technological uses.

In the absence of a magnetic field, the plasma/wall transition is split into two main regions, i.e., the non-neutral sheath and the quasi-neutral collisional pre-sheath. The sheath region is known to scale with the Debye length λ_d, while the relevant characteristic length for the pre-sheath can be for instance the collision mean-free-path with neutrals λ_c, or the minimum of the various collision mean-free-paths (ionization, recombination, charge-exchange, etc.) which are relevant to describe the physics of the pre-sheath region.

It has been shown based on a fluid model that, in order to prevent an oscillatory potential distribution at the sheath edge,

ion velocity, perpendicular to the wall V_{ix}, must verify what is known as the Bohm criterion[4]

$$V_{ix} > C_s = \sqrt{\frac{T_e + T_i}{M}}, \tag{1}$$

where C_s is the ion sound velocity, T_e and T_i are the electron and ion temperature, respectively, and M is the ion mass.[5,6] Note that in this paper, temperatures will be expressed in energy units only. This sound velocity is also the critical velocity at which quasi-neutrality breaks down in the pre-sheath region[7] (the plasma approximation stands as long as $V_{ix} < C_s$) so that it is usually assumed that the Debye sheath entrance is located at the sonic point S, where $V_{ix} = C_s$. Neglecting inertia for electrons ($m = 0$, where m is the electron mass) and ionization within the sheath region, assuming equal ion and electron losses at the wall and using Eq. (1), it is possible to calculate the potential drop between the wall and the sheath edge as

$$\Delta\phi_d = \frac{T_e}{2e} \ln\left[2\pi \frac{m}{M}\left(1 + \frac{T_i}{T_e}\right)\right], \tag{2}$$

which is usually a negative quantity.

In the presence of a magnetic field tilted by θ with respect to the wall, another sonic point can be derived from the fluid equations. First evidenced by Chodura,[8] an additional quasi-neutral region appears between the Debye sheath and the collisional pre-sheath, where ions are accelerated from $V_{ix} = C_s \sin\theta$ to C_s, i.e., from a point C where the projection of the ion velocity along the field line, $V_{i\parallel} = C_s$, to the point S where the component is perpendicular to the wall, $V_{ix} = C_s$.

This region, usually called the "Chodura sheath" or "magnetic pre-sheath," scales with the ion Larmor radius R.[9] However, when the plasma is collisional enough, if the ion mean-free-path λ_{ci} is smaller than R, despite the preferential direction of the magnetic field, the plasma flow is isotropized by frequent collisions during the ion cyclotronic period. Some authors have shown that in such a high collisional case, the Chodura sheath disappears and overlaps with the collisional pre-sheath, leading to a classical double layer structure for the PWT.[10,11] Other studies emphasized the role of the magnetic field angle and strength on the different regions since the original work of Chodura.[12,13]

The potential drop in the Chodura sheath $\Delta\phi_{cho}$, between point C and point S, can be easily calculated by neglecting (like previously for the Debye sheath) the particle source and electron inertia as

$$\Delta\phi_{cho} = \frac{T_e}{e} \ln(\sin\theta), \tag{3}$$

which is also a negative quantity.

Interestingly, as pointed out by Stangeby et al.,[14] the potential drop between the Chodura sheath entrance (point C) and the wall, which we call $\Delta\phi_T$, is strictly equal to Eq. (2)

$$\Delta\phi_T = \Delta\phi_{cho} + \Delta\phi_d = \frac{T_e}{2e} \ln\left[2\pi \frac{m}{M}\left(1 + \frac{T_i}{T_e}\right)\right], \tag{4}$$

which is the total potential drop in the Debye and the Chodura sheaths. It is expected to be independent on the incidence of the magnetic field as long as one can assume strongly magnetized electrons (barely drifting from their field line) and neglect their inertia. Then, for a critical angle θ^*, the Debye sheath disappears ($\Delta\phi_d = 0$). It comes from (3) and (4)

$$\sin\theta^* = \sqrt{2\pi \frac{m}{M}\left(1 + \frac{T_i}{T_e}\right)}. \tag{5}$$

Below θ^* (of the order of 9.12, 6.43, and 4.75° for $M/m = 500$, 1000, and 1836, respectively, and assuming $T_i = T_e$), quasi-neutrality does not break down anymore and the Bohm criterion given by Eq. (1) is not fulfilled. Stangeby[15] inferred that below θ^* the potential drop in the Chodura sheath still equals Eq. (4) as long as $\theta \geq \sqrt{m/M}$ and estimated the ion fluid velocity at the wall (at the Chodura sheath exit) as proportional to $\sin\theta$. This tendency has been checked against kinetic simulations, where it was shown that charge separation progressively vanishes for grazing incidence, with the ion flow velocity limited to subsonic speeds.[16] However, these kinetic simulations were performed with electrons following a Boltzmann law so that their inertia was not taken into account, leading to a possible discrepancy at grazing incidences. This regime of very grazing incidence, where $\theta < \theta^*$, despite its strong implication in tokamaks, for instance, has never been deeply investigated for inertial electrons and in the presence of collisions.

Note that in the limit of $\theta \to 0$, in a 1d/3V description of the plasma, the particle flux at the wall is expected to cancel in the collisionless limit because particles cannot drift perpendicular to the field line. Some authors have addressed this quasi-static issue theoretically and by using particle-in-cell (PIC) simulations.[17–24] They showed that the potential drop at the vicinity of the surface is opposite, i.e., ions are pushed back into the plasma instead of being accelerated towards the walls, the space charge being negative, due to the larger Larmor radius of the ions (vs. the electrons one). Collisions can restore the particle current perpendicular to the field line though, for $\theta = 0$, and the potential drop sign will then depend on the mean-free-path to Larmor radius ratio.[25]

In this paper, we investigate by means of PIC simulations, without assuming the Boltzmann electron response, the evolution of different potential drops in the PWT with respect to both the angle of incidence of the magnetic field and the charged particles vs. neutrals collision rates. In the first part of this paper, after a description of the geometry of the studied system and a general overview of the PIC code, potential and velocity spatial profiles, followed by the potential drops in the PWT, are presented for a large range of the mean-free-path to Larmor radius ratios. In the second part, we review the fluid models allowing the derivation of points C and S; we also include the electron inertia in order to extrapolate potential drops at very grazing incidences and derive a modified Bohm criterion. We show that for large θ, the simulated potential drop in the combined collisional pre-sheath and Chodura sheath follows its expected fluid angular variation. We also show that at a critical incidence angle given by $\theta_c = \arcsin\frac{R}{\lambda_{ci}}$, when $\lambda_{ci} > R$, particle flows depend on

collisions just as in the high collisionality case when $\lambda_{ci} < R$. Potential drops in the quasi-neutral region, calculated by using a collisional model, reproduce fairly well the simulated ones when $\theta < \theta_c$ or $\lambda_{ci} < R$.

II. PIC SIMULATIONS

The studied system is in a one dimensional plasma bounded by two conductive walls, separated by $200\lambda_d$, with the origin of the x axis in the center of the plasma, as depicted in Fig. 1. The magnetic field, of strength B, is tilted by θ with respect to the wall in the (Oz) direction. The 1d3V PIC code used for the simulations was developed in the laboratory by the authors.[24] The simulation cell size is chosen as $0.1 \times \min(r, \lambda_d)$, where r is the electron Larmor radius, in order to describe with a sufficient accuracy the motion of both ions and electrons. For all the simulations presented in this study, we choose $T_i = T_e = 2\,\mathrm{eV}$, which are temperatures representative of plasma discharges.[26] The simulations are also run with a reduced ion mass, such as $M/m = 500$. This choice is motivated by computational time issues: in order to describe properly the evolution of different potential drops in the PWT with respect to the angle of incidence of the magnetic field, a large number of simulations have to be envisaged. The total simulation time scales with the ion cyclotronic period, while the simulation time step scales with the electron one so that the total number of iterations scales with the ion-to-electron mass ratio. Although the present study can be extended to the realistic mass ratio for, e.g., H^+, He, or Ar, provided a significant investment in computing power, the present value of $M/m = 500$ is a reasonable trade-off.
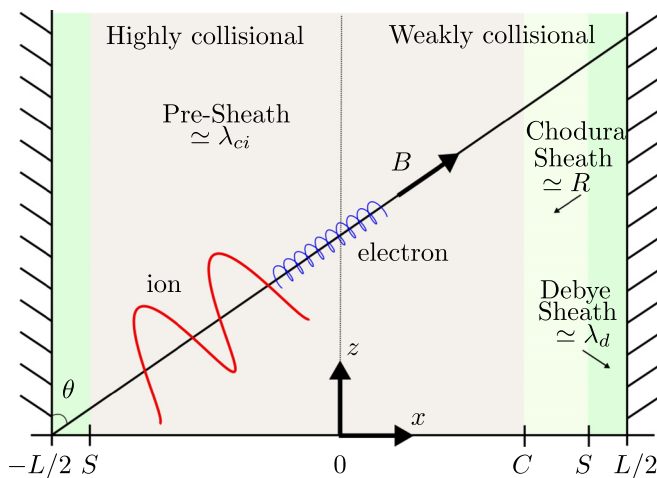
FIG. 1. Sketch of the one dimensional plasma studied, depicting two extreme collisional cases. On the left, the expected layers in the high collisionality regime are the Debye sheath and the collisional pre-sheath. On the right, in the low collisionality mode, three layers are expected, where the Chodura sheath takes place between the de Debye one and the pre-sheath. Each layer scales with its proper characteristic length. The walls are located at the abscissa $-L/2$ and $L/2$ and grounded in the PIC simulations. C and S are the sonic point locations. The electron and ion trajectories, drawn in red and blue, respectively, are not representative of the real motion of particles, especially in the presence of collisions, where particles undergo a random-walk.

With a magnetic field $B = 0.05\,\mathrm{T}$, we have $r/\lambda_d = 0.9$, so we can consider that electrons are moderately magnetized. However, as will be shown in the following in the model used to interpret the PIC simulations results, they barely drift from their field line, even for such an average ratio. Initially, the superparticles are uniformly distributed on the grid and their velocity chosen randomly from Maxwellian distributions, whose nominal temperatures are T_i and T_e. During the simulation runs, the number of ions is kept constant by the following method: at each time step, couples (ion + electron) are injected at random positions in the plasma, in order to compensate for the number of ions lost at both walls during the previous time step.

The charged particles undergo collisions with the neutrals. We have developed a simple operator, which conserves the total kinetic energy and the total momentum, assuming particles as hard spheres, with a cross-section independent of the velocity. A complete description of the collisional model is given in Ref. 25. Note that within this hard sphere model, assuming ions and neutrals of identical diameter, the ion mean-free-path $\lambda_{ci} = \lambda_{ce}/4$, with λ_{ce} the electron one. Such a hard sphere model for the charged particles vs. neutral collision is a crude approximation. In real systems, other collisional processes, charge-exchanges or excitations, dominate and have to be taken into account in the numerical model if an accurate description of the atomistic physics is expected (see, for instance, Ref. 27). The aim of our simulations is however to understand the qualitative effect of collisions onto the PWT structure and more particularly to understand how the collisional redistribution of velocities affects the dynamics of the particles at the vicinity of the walls and, consequently, the potential drops in the PWT. To emphasize the role of collisions, we choose to express the ion and electron mean-free-paths in Larmor radius units, which measures the importance of the anisotropy due to the magnetic field, independent of the atomistic nature of the collisions.

It is also important to note here that this collisional model makes faster particles have higher probability to collide (the cross-section being independent of the velocity). Moreover, the injection method used, which is known to distort the velocity distribution functions,[28–30] induces a cooling of the plasma with respect to the nominal loaded one. That is why the real temperature of the charged particles to which we normalize potential drops and velocities at the end of the simulations are extracted from the PIC simulations via a Maxwellian fit of the velocity distribution functions.

The electron mean-free-path λ_{ce} is set such that electrons are not demagnetized by collisions, within the range $10 < \frac{\lambda_{ce}}{r} < 750$. As previously explained, the ion one is 4 times smaller; therefore, using the nominal temperatures and the mass ratio, it satisfies the ordering $0.1 < \frac{\lambda_{ci}}{R} < 8.3$. This range of the ion mean-free-path allows the study of the transition between a highly collisional regime, where the magnetic field effect onto ion motion is canceled by collisions, and an anisotropic one, where the ion flow has to follow the field line. This transition can be seen on the spatial potential and velocity profiles as depicted in Fig. 2.
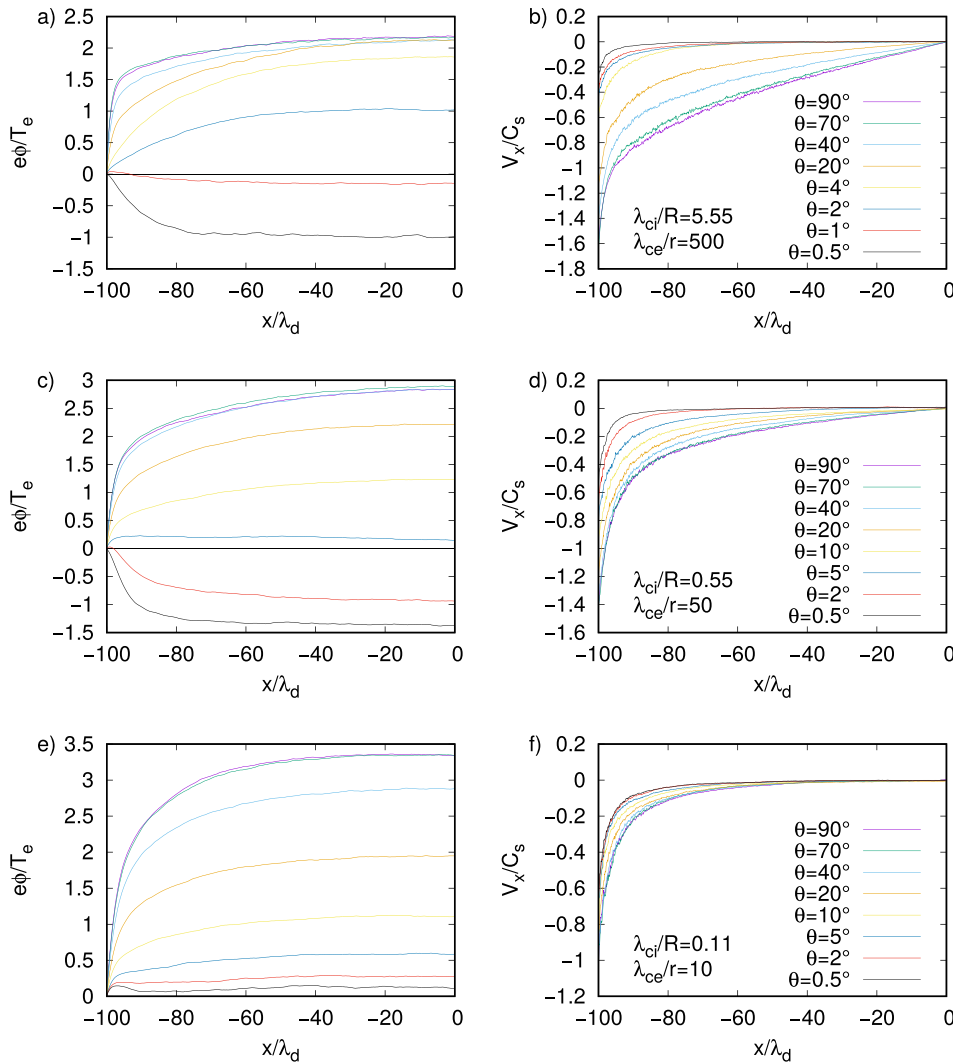
FIG. 2. Left: normalized potential profiles for 3 different mean-free-path to Larmor radius ratios and 8 values of the angle of incidence of the magnetic field θ. Right: corresponding ion velocity profiles normalized to the sound velocity.

In the very high collisional case ($\lambda_{ce}/r = 10$ and $\lambda_{ci}/R = 0.11$), the magnetic field incidence does not change the ion velocity flow qualitatively [see Fig. 2(f)]: the subsonic flow is isotropic for ions and the potential in the plasma is always positive, so ions are accelerated towards the collecting surface for any θ as depicted in Fig. 2(e). For intermediate neutral gas density, $\lambda_{ce}/r = 50$ and $\lambda_{ci}/R = 0.55$, the effect of the magnetic field begins to influence the ion flow as seen in Fig. 2(d). In that case, for grazing incidences of the magnetic field, when $\theta < 5°$, the opposite situation to that previously arises since it is necessary to push back ions into the plasma [the potential drop between the wall and the plasma is inverted in Fig. 2(c)]. This situation has already been evidenced in the case of a magnetic field parallel to the wall.[25] For larger incidences though, the potential drop between the wall and the center of the plasma column reaches $-2.9T_e/e$ for $\theta = 90°$ and the ion flow is supersonic for

$\theta \geq 20°$. The inversion of the potential drop between the wall and the center of the plasma can also be seen on the space charge profiles in Fig. 3(a) for $\lambda_{ci}/R = 0.55$. The space charge amplitude decreases with θ as already pointed out in Ref. 16, and for $\theta = 0.5°$, the space charge is alternatively positive close to the wall and negative towards the plasma, as in the case of a perfectly aligned magnetic field.[25] It also leads to an inversion of the electric field E polarity as shown in Fig. 3(b), where ions are accelerated towards the wall for $\theta \geq 5°$ and pushed back into the plasma for very grazing incidences otherwise.

Finally, when both ions and electrons are magnetized (i.e., $\lambda_{ce}/r = 500$ and $\lambda_{ci}/R = 5.5$), there is a strong dependence of the ion velocity flow on the magnetic field incidence [Fig. 2(b)]. It stays supersonic at the vicinity of the wall for $\theta > 20°$, and the velocity at the exit of the plasma decreases
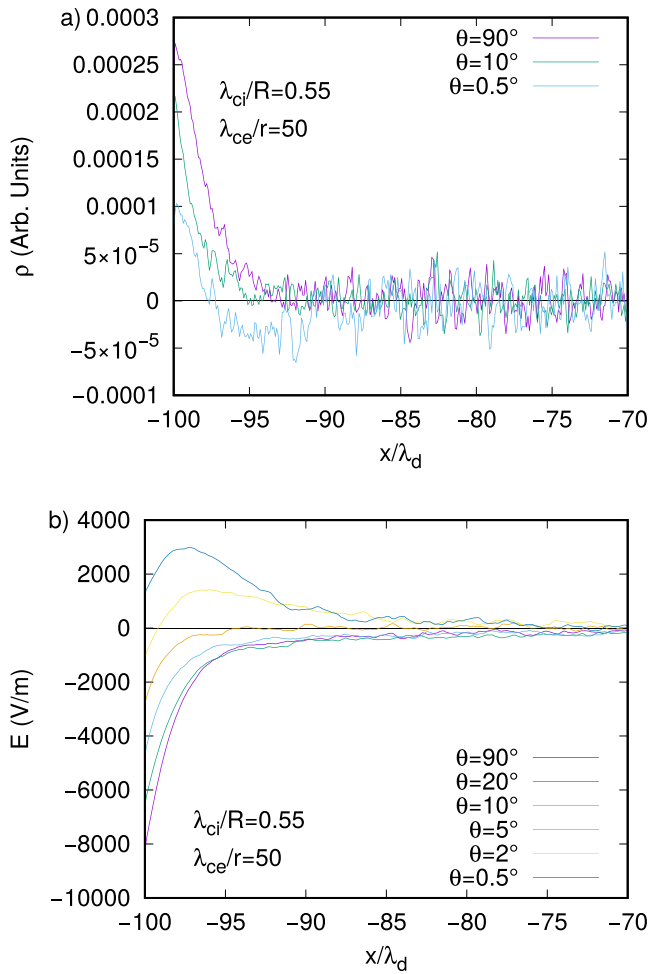
FIG. 3. (a) Space charge at the vicinity of the left wall for 3 angles of incidence and a medium collisionality of the ions ($\lambda_{ci}/R = 0.55$). (b) Electric field profiles for the same mean-free-path to Larmor radius ratio as in (a) for 6 angles of incidence of the magnetic field.

slowly with θ [see also Fig. 7(b)]. The same observation on the potential profiles in Fig. 2(a) can be done as previously although the potential drop between the wall and the plasma center reaches $-2.17 T_e/e$ for large incidences. This is slightly smaller than for $\lambda_{ci}/R = 0.55$ in Fig. 2(c), which, we infer, is due to the lower collisionality (it is more difficult to increase the velocity flow, when the friction is more important, so a larger potential drop is required).

In order to define the potential drops in the different parts of the PWT, we use a simple criterion that can be applied to all PIC results: we consider that the Debye sheath entrance is located at the sonic point S, where $V_{ix} = C_s$. If the ion velocity flow does not reach the sonic point, we assume that the Debye sheath disappears and $\Delta\phi_d = 0$. Otherwise, the spatial coordinate of S is obtained from V_{ix}, for instance, from Fig. 2(b), and the corresponding potential value $\phi(s)$, from the normalized potential profile [e.g., Fig. 2(a)].
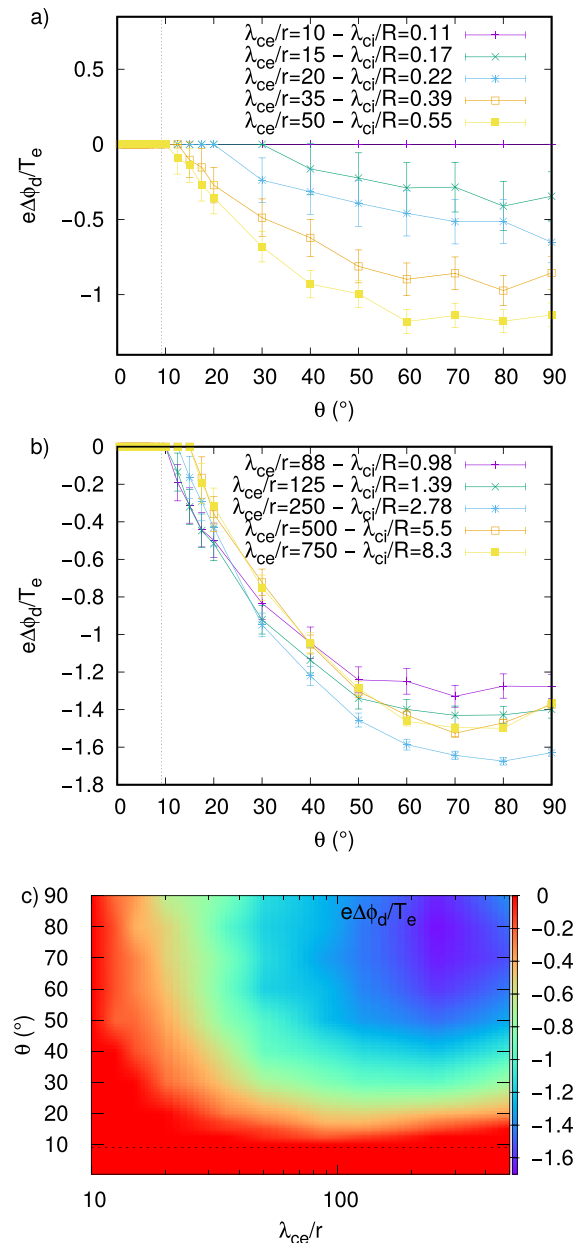
FIG. 4. Normalized potential drop $\Delta\phi_d/T_e$ in the Debye sheath against the incidence of magnetic field θ for different mean-free-path to Larmor radius ratios. In (a), the high collisionality makes the ion velocity flow isotropic, while in (b), both ions and electrons are magnetized. The dotted line is at the abscissa $\theta = \theta^*$ given by Eq. (5). (c) Density plot of $\Delta\phi_d/T_e$ vs. θ and λ_{ce}/r.

Figure 4 shows the potential drop within the Debye sheath against θ for different mean-free-path to Larmor radius ratios. In the very high collisionality case, for $\lambda_{ce}/r = 10$, i.e., $\lambda_{ci}/R = 0.11$, the ion velocity flow does not reach C_s, and there is no Debye sheath [Fig. 4(a)]. In this case, the whole potential drop between the wall and the center of the plasma

is in the collisional pre-sheath, which is quasi-neutral. For larger mean-free-paths in Figs. 4(a) and 4(b), $\Delta\phi_d$ increases with λ_{ce}/r until its saturation for $\lambda_{ce}/r > 88$ ($\lambda_{ci}/R > 0.98$) in the medium-low collisionality regime of the ions. In this case, a high space-charge electric field is required to balance ion and electron losses at the walls.

Using Eq. (4) with the nominal plasma parameters, it comes that for $\theta \rightarrow \pi/2$, $e\Delta\phi_d/T_e \rightarrow -1.84$, which is comparable to the simulation results in Fig. 4(b), $e\Delta\phi_d/T_e \simeq -1.4$ for the lowest collisionality [as mentioned previously, the plasma temperature is usually colder than its nominal value at the end of the simulation runs due to the particle injection procedure: this can explain the small discrepancy between the expected value and the simulations one; formula (4) should be used with the temperatures of each simulation run]. The dotted line in Fig. 4 represents the critical angle $\theta\star$, given by Eq. (5), where the Debye sheath is expected to disappear based on the fluid model. $\theta\star$ is always a bit smaller (in the range $3 - 5°$) than the angle at which $\Delta\phi_d$ really vanishes due to collisions. This can also be seen in Fig. 4(c), which is a density plot representing the potential drop in the Debye sheath vs. θ and λ_{ce}/r. The red color indicates the region where the Debye sheath vanishes. We observe that both grazing incidence and high collisionality are responsible of its disappearance. This density plot was obtained by an interpolation of our numerical results, which in large part are shown in Figs. 4(a) and 4(b).

Note that the error bars in Fig. 4, as well as in the following figures, are calculated based on two sources of error. The potential profiles are obtained by averaging the signal in time over several ion cyclotronic periods (just as the velocity profiles or the densities), so it is possible to calculate the standard error of the mean, which is the first source of error. The second one is simply based on the extraction procedure explained previously, when searching for the Debye sheath entrance. This location cannot be known at a better precision than the grid step size, which is, with our magnetic field strength, $0.1 \times r$. This gives finally an uncertainty on the potential values.

Once the sonic point S is determined, and its potential value $\phi(S)$ is read, one can extract the potential drop in the quasi-neutral region, $\Delta\phi_{qn}$ as $\phi(S) - \phi(0)$, where $\phi(0)$ is the potential at the center of the plasma. If the plasma does not reach the Bohm velocity, $\phi(S) = \phi(-L/2) = 0$, and the potential drop in the quasi-neutral region consists of the total potential variation between the grounded wall and the center of the plasma (which happens for high collisionality or grazing incidence such as $\theta < \theta\star$).

The quasi-neutral region can be a collisional pre-sheath only if $\lambda_{ci} < R$. Otherwise, it is composed of the Chodura sheath and a collisional pre-sheath as depicted in Fig. 1. Figures 5(a) and 6(a) show the potential drop $e\Delta\phi_{qn}/T_e$ with respect to the angle θ in the two extreme cases of low and high collisionality, respectively. When $\lambda_{ce}/r > 250$ (i.e., $\lambda_{ci}/R > 2.77$), in Fig. 5(a), $\Delta\phi_{qn}$ does not vary anymore with the mean-free-path for $\theta > 20°$. For comparison, we plot in the same figure the collisionless case which does not deviate
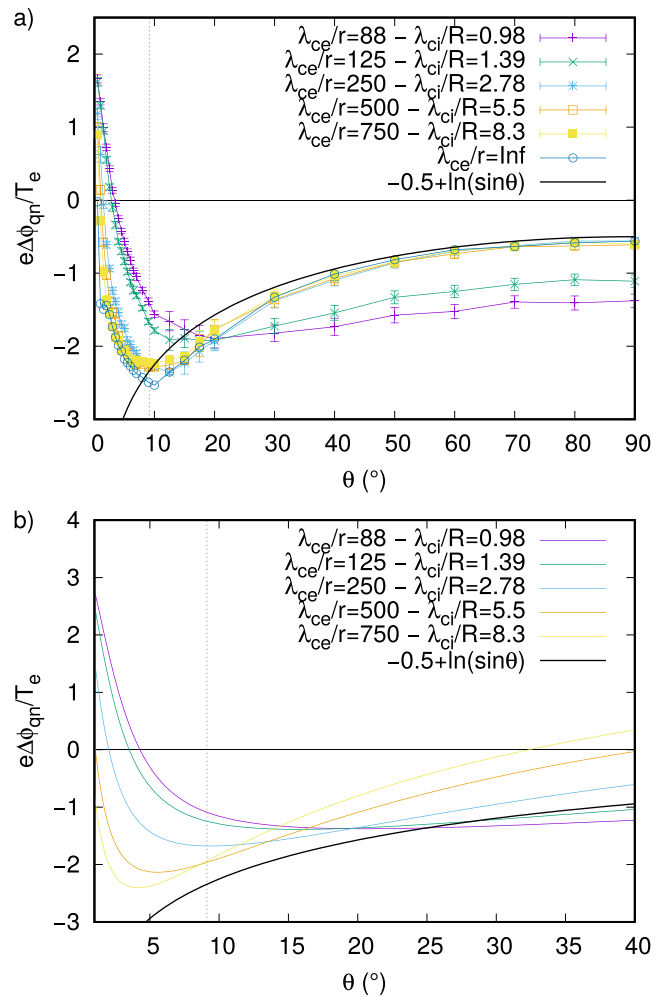
FIG. 5. (a) Normalized potential drop $e\Delta\phi_{qn}/T_e$ in the quasi-neutral region vs. the angle of incidence of the magnetic field in the medium-low collisionality regime of the ions. (b) Theoretical $e\Delta\phi_{qn}/T_e$, Eq. (33), in the context of a high collisionality approximation.

from the low collisional ones ($\lambda_{ce}/r = 250$, 500, or 750). On the other hand, below $\theta = 20°$, a slight difference occurs between the various curves; more particularly, it can be seen that the change in the sign of $\Delta\phi_{qn}$ appears at angles which decrease with increasing λ_{ce}/r. In the high collisional case, the potential drop in the quasi-neutral region (i.e., the collisional pre-sheath) is very sensitive to the ratio λ_{ce}/r. The smaller it is the larger both the collisionality and potential drop are [see Fig. 6(a)]. The sign of $\Delta\phi_{qn}$ also changes at grazing incidences, but for larger angles than in the low collisional case.

Finally, we have extracted the Chodura point location C from the velocity profiles, as we did for the sonic point S, and calculated the total potential drop in the combined Chodura and Debye sheaths $\Delta\phi_T = \Delta\phi_d + \Delta\phi_{cho}$, which is expected to stay constant, independent of the angle of
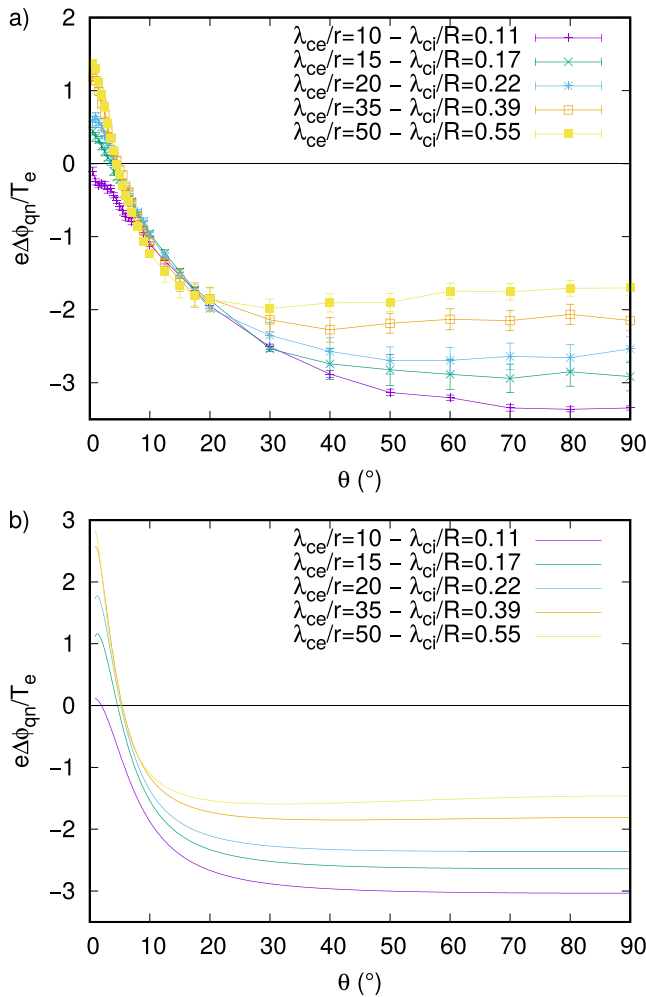
FIG. 6. (a) Normalized potential drop $e\Delta\phi_{qn}/T_e$ in the quasi-neutral region vs. the angle of incidence of the magnetic field in the high collisionality regime of the ions. (b) Theoretical $e\Delta\phi_{qn}/T_e$, Eq. (33), for the same mean-free-path to Larmor radius ratios than in (a).

incidence of the magnetic field [see Eq. (4)]. Figure 7(a) shows $\Delta\phi_T$ vs. θ for different mean-free-path to Larmor radius ratios, only in the case $\lambda_{ci} \geq R$. For $\theta > 20°$, the total potential drop keeps a constant value, close to the expected one. However, for grazing incidences, in contrast to Stangeby assumptions,[15] $\Delta\phi_T$ varies with the magnetic field incidence (specifically around and below $\theta*$), rapidly decreasing and even becoming positive at very low incidences of the order of a few degrees.

In order to explain all these features, and more particularly the behavior of the potential drops in the PWT for grazing incidences, we expanded the fluid models, inspired by Ahedo's study,[10] taking into account both the magnetic field and collisional effects on ion fluid velocity, as well as electron inertia.
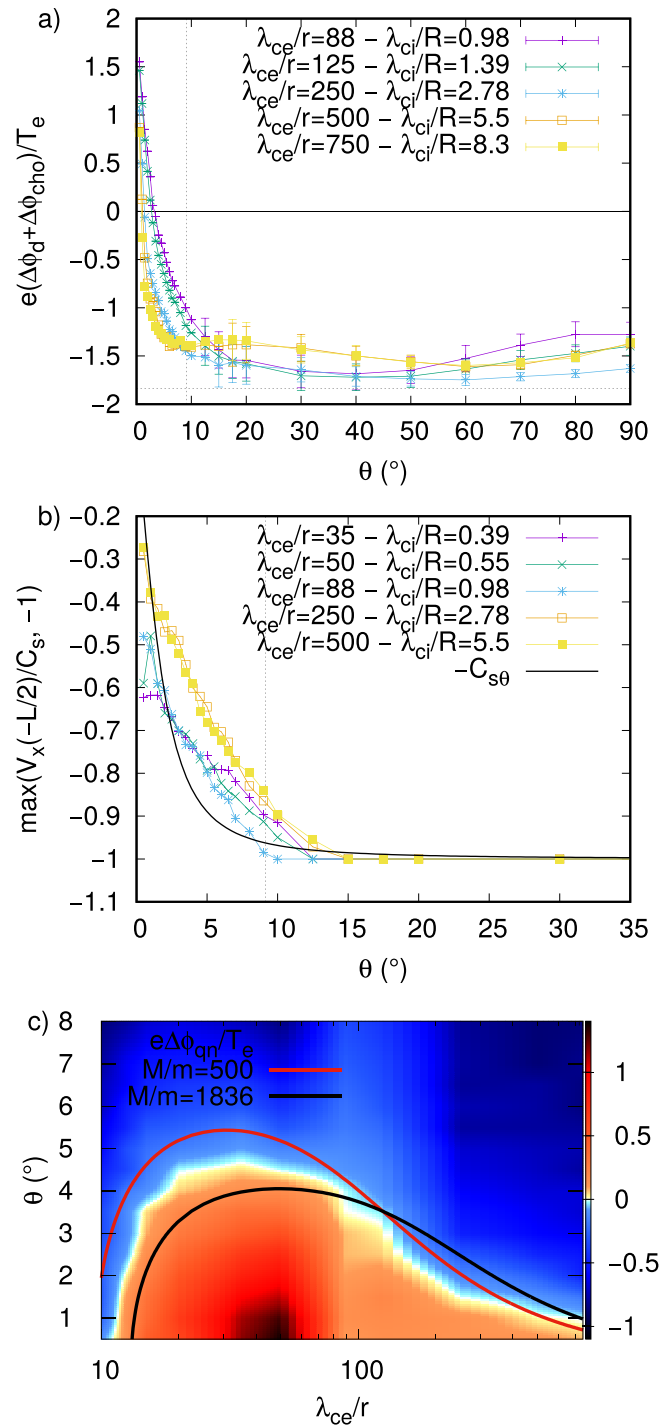
FIG. 7. (a) Normalized potential drop $e\Delta\phi_T/T_e$ in the combined Debye and Chodura sheaths vs. the angle of incidence of the magnetic field in the medium-low collisionality regime of the ions. (b) Variation of the velocity at the exit of the quasi-neutral region, which can be the Bohm velocity C_s or the velocity at the wall $V_x(-L/2)$, normalized to C_s. (c) Normalized potential drop in the quasi-neutral region vs. θ and the mean-free-path to Larmor radius ratio for grazing incidences only. The straight lines are the critical angles θ_p plotted using Eq. (35) for two mass ratios with $T_i = T_e$.

III. FLUID MODEL FOR THE QUASI-NEUTRAL REGION
A. Velocity field in the presence of B and collisions with neutrals

The magnetic $\vec{B}$ and electric field $\vec{E}$ components are $B \times (\sin\theta, 0, \cos\theta)$ and $E \times (1, 0, 0)$, respectively.

In the steady state, the fluid equations of momentum conservation on the x, y, and z components, denoting the derivative in x by a prime symbol, are

$$n\mu V_x V_x' = -nq\phi' + nqV_yB\cos\theta - n'T - n\mu\nu V_x, \quad (6)$$

$$n\mu V_x V_y' = -nqV_xB\cos\theta + nqV_zB\sin\theta - n\mu\nu V_y, \quad (7)$$

$$n\mu V_x V_z' = -nqV_yB\sin\theta - n\mu\nu V_z. \quad (8)$$

This system describes both ions and electrons, where μ, n, ν, and q are the mass, density, collision frequency, and electric charge of the considered species, respectively. This set of equations can be rewritten in a more convenient way, which highlights the different lengths of the system

$$\frac{V_x V_x'}{V_t^2} = -\frac{q\phi'}{T} + \frac{V_y}{V_t}\frac{\cos\theta}{\lambda_m} - \frac{n'}{n} - \frac{V_x}{V_t}\frac{1}{\lambda_c}, \quad (9)$$

$$\frac{V_x V_y'}{V_t^2} = -\frac{V_x}{V_t}\frac{\cos\theta}{\lambda_m} + \frac{V_z}{V_t}\frac{\sin\theta}{\lambda_m} - \frac{V_y}{V_t}\frac{1}{\lambda_c}, \quad (10)$$

$$\frac{V_x V_z'}{V_t^2} = -\frac{V_y}{V_t}\frac{\sin\theta}{\lambda_m} - \frac{V_z}{V_t}\frac{1}{\lambda_c}, \quad (11)$$

where $V_t = \sqrt{\frac{T}{\mu}}$ is the thermal velocity and λ_m and λ_c are the Larmor radius and mean-free-path of the considered species, respectively. Neglecting ionization or recombination, the conservation of the particle number yields

$$\frac{\partial(nV_x)}{\partial x} = 0. \quad (12)$$

Extracting V_z of Eq. (11), substituting it in Eq. (10), as well as V_y from Eqs. (10) to (9), and using Eq. (12) lead to

$$\frac{V_x'}{V_t} - \frac{V_x'V_t}{V_x^2} = -\frac{q\phi'V_t}{TV_x} - \frac{\cos\theta}{\frac{\lambda_m^2}{\lambda_c^2} + \sin^2\theta}\left(\frac{V_y'}{V_t}\frac{\lambda_m}{\lambda_c} + \frac{V_z'}{V_t}\sin\theta + \frac{\cos\theta}{\lambda_c}\right) - \frac{1}{\lambda_c}. \quad (13)$$

In the case of low collisionality ($\lambda_m \ll \lambda_c$) and when $\sin\theta \gg \frac{\lambda_m}{\lambda_c}$, Eq. (13) can be simplified as

$$V_x'\left(1 - \frac{V_t^2}{V_x^2}\right) = -\frac{q\phi'}{\mu V_x} - \frac{V_z'}{\tan\theta} - \frac{V_t}{\lambda_c \sin^2\theta}. \quad (14)$$

Using the same ordering of the characteristic lengths, one can see from Eqs. (10) to (11) that, in regions with the gradient scale length λ_c, $V_y \ll V_z$ and $V_x \simeq V_z \tan\theta$. Equation (14) becomes

$$\mu V_x V_x'\left(\frac{1}{\sin^2\theta} - \frac{V_t^2}{V_x^2}\right) = -q\phi' - \mu\frac{V_x V_t}{\lambda_c \sin^2\theta}. \quad (15)$$

If the previous ordering is valid for both ions and electrons, then the plasma moves along the magnetic field line only.

Equation (15) is the momentum conservation equation along the magnetic line projected onto the x axis.

For an incidence of the magnetic field such as $\sin\theta \simeq \frac{\lambda_m}{\lambda_c}$, a component perpendicular to the magnetic line appears in the velocity field, and the previous approximations do not stand any more. This critical angle has already been derived in Ref. 30 with a similar assumption concerning the fluid velocity field although these authors consider only incidences larger than this critical one. It is possible to consider then, when the plasma is quasi-neutral, that the plasma velocity is smaller than the thermal one so that inertial terms in Eqs. (9) to (11), quadratic in velocity, can be neglected.

Finally, in the high collisional regime, where $\lambda_c < \lambda_m$, one can neglect the inertial part of Eqs. (10) and (11) (left members), which are quadratic in velocity. With the previous ordering of the mean-free-path and of the Larmor radius, one can see from Eqs. (11) to (10) that V_z and V_y are negligible. Collisions overcome the magnetic order, and as the electric field is on the x-axis in our one dimensional model, there is only a net drift in this direction, while the average velocities in both y and z directions are null: Eq. (9) describes in this case a diffusive motion along the x axis only.

B. Bohm criterion for strongly magnetized electrons

Let us assume that the ion velocity field follows Eq. (9) which stands for any collisionality. Let us further assume $\sin\theta \gg \frac{r}{\lambda_{ce}}$ so that Eq. (15) describes electron momentum conservation for any mean-free-path but not necessarily ion momentum conservation because $\sin\theta$ can be larger or smaller than $\frac{R}{\lambda_{ci}}$. In the plasma, far from the sheaths, the plasma approximation stands, and we have $n_i \simeq n_e \simeq n$, where n_i and n_e are the ion and electron densities, respectively. It comes that $V_{ex} \simeq V_{ix} \simeq V_x$, where V_{ex} is the electron velocity perpendicular to the wall. Substituting the electric force $q\phi'$ from Eqs. (15) into (9) and using Eq. (12), with electron and ion parameters for the mass, temperature, Larmor radius, and mean-free-path, yields

$$\frac{M\sin^2\theta + m}{T_i\sin^2\theta}\frac{V_x'}{V_x}\left(V_x^2 - C_{s\theta}^2\right) = \frac{V_{iy}\cos\theta}{V_i R}$$
$$- \frac{V_x}{V_i}\left(\frac{V_e m}{V_i M}\frac{1}{\lambda_{ce}\sin^2\theta} + \frac{1}{\lambda_{ci}}\right), \quad (16)$$

with the modified Bohm velocity

$$C_{s\theta} = \frac{C_s\sin\theta}{\sqrt{\sin^2\theta + m/M}} \quad (17)$$

and V_i and V_e defined as the ion and electron thermal velocity, respectively.

The modified Bohm velocity takes into account electron inertia that becomes important for grazing incidences when $\theta \simeq \sqrt{m/M}$ as already mentioned by Stangeby in Ref. 15. Then, as long as electrons are moving along the field line (for $\lambda_{ce} \gg r$), even if their inertia matters, the quasi-neutrality breaks down at the modified Bohm velocity, which is very close to C_s for large

incidences, but vanishes as $\theta \simeq 0$. This result does not depend on the collisionality of the ions, and their velocity field could be isotropic for $\lambda_{ci} < R$ or anisotropic when the magnetic effects overcome collisions.

C. Low collisionality $\lambda_{ci} \gg R$

In regions that scale with λ_{ci} and when the angle of incidence of the magnetic field is such that $\sin \theta > \frac{R}{\lambda_{ci}}$, ions also verify Eq. (15), such as electrons. Combining both equations and eliminating the electric field force give

$$\frac{m+M}{\sin^2\theta}\frac{V_x'}{V_x}\left(V_x^2 - \frac{T_e+T_i}{m+M}\sin^2\theta\right) = -\frac{V_x}{\sin^2\theta}\left(\frac{mV_e}{\lambda_{ce}} + \frac{MV_i}{\lambda_{ci}}\right). \quad (18)$$

In order to get a positive gradient of the velocity, one must have

$$V_x < \sqrt{\frac{T_e+T_i}{m+M}}\sin\theta \simeq C_s \sin\theta, \quad (19)$$

which is known as the Chodura sheath entrance condition. As already pointed out by Ahedo,[10] at this specific sonic point, the plasma enters a steeper region of scale R, where it stays quasi-neutral until it enters the Debye sheath at the sonic point $V_x = C_{s\theta}$.

D. High collisionality $\lambda_{ci} \ll R$ or incidences such as $\sin \theta < \frac{R}{\lambda_{ci}}$

When the angle of incidence of the magnetic field is smaller or of the same order of magnitude than $\theta_c = \arcsin\frac{R}{\lambda_{ci}}$, it is not possible to neglect the collisional term in Eq. (10) or Eq. (11) vs. the magnetic ones. The inertial terms can be disregarded though, for velocities smaller than the thermal one. This situation corresponds geometrically to the interception of the ion Larmor radius with the wall at a distance λ_{ci} from it along the field line. In such a case, the Chodura sheath, which extends over some R in front of the wall, becomes collisional, even if $\lambda_{ci} > R$, and tends to disappear and merge with the collisional pre-sheath.

For $\lambda_{ci} \ll R$, condition (19) vanishes and so does the Chodura sheath (ions are demagnetized by collisions), and one can see from Eqs. (10) to (11) that, as already mentioned, $V_{iz} \simeq V_{iy} \ll V_{ix}$.

In both situations described in this section, Eq. (16) and the modified Bohm criterion given by Eq. (17) still hold. The important conclusion is that the Chodura sheath merges with the collisional pre-sheath for $\lambda_{ci} < R$ and for incidences such as $\sin \theta < \frac{R}{\lambda_{ci}}$.

E. Potential drop in the quasi-neutral region

1. $\lambda_{ci} \gg R$

For θ larger than both θ_c and θ^* and low collisionality, one can neglect electron inertial effects. Indeed, dividing

successively Eq. (15) for electrons by m and then by V_e^2, using Eq. (12), yields

$$\frac{V_x V_x'}{V_e^2 \sin^2\theta} + \frac{n'}{n} = \frac{e\phi'}{T_e} - \frac{V_x}{V_e}\frac{1}{\sin^2\theta\lambda_{ce}}. \quad (20)$$

Assuming the electron fluid velocity smaller than V_e, i.e., $V_x/V_e \ll 1$, and large incidences of the magnetic field, yields the Boltzmann relation from Eq. (20)

$$\frac{n'}{n} = \frac{e\phi'}{T_e}. \quad (21)$$

The Boltzmann relation (21) can also be derived directly from Eq. (9) assuming that $V_{x,y,z} \ll V_e$ for $\theta > \theta^*$. Noting the potential at the Debye and Chodura sheath entrance as ϕ_d and ϕ_c, respectively, it comes from Eq. (21) that $\frac{n_d}{n_c} = \exp\frac{e(\phi_d - \phi_c)}{T_e}$, with n_d and n_c being the plasma density at the latter entrances. Knowing the velocity at both sonic points, it is straightforward to calculate the well-known potential drop in the Chodura region using Eq. (12) as

$$\Delta\phi_{cho} = \phi_d - \phi_c = \frac{T_e}{e}\log(\sin\theta). \quad (22)$$

In order to get the total potential drop in the quasi-neutral region $\Delta\phi_{qn}$, one has to evaluate the potential at the Chodura point, assuming $\phi(0) = 0$ and $V_x(0) = 0$. As explained previously, for such an ordering of different characteristic lengths, the plasma flows parallel to the field line (ions and electrons). So, for every angle, the plasma has to be accelerated from an expected null velocity at $x = 0$ to C_s at $x = C$ along the field line (or $C_s \sin\theta$ in the x direction).

Using Eq. (15) for ions and Eq. (12) and neglecting the collisional drag, we have

$$\frac{n'}{n} = -\frac{e\phi'}{T_i} - \frac{MV_x V_x'}{T_i \sin^2\theta}, \quad (23)$$

which can be substituting in Eq. (21). After integration between the Chodura sheath entrance and the plasma center, it comes that $\phi_c - \phi(0) = -0.5T_e$, which is independent of the magnetic field incidence.

The total potential drop in the quasi-neutral region is then, for $\theta > \theta^*$ and $\theta > \theta_c$,

$$\Delta\phi_{qn} = \frac{T_e}{e}\left(\log(\sin\theta) - 0.5\right). \quad (24)$$

In Fig. 5(a), we observe that Eq. (24) fits qualitatively the PIC simulations results for incidences larger than 20° as long as $\lambda_{ce}/r \geq 250$. Note that the values of $\theta_c = \arcsin\frac{R}{\lambda_{ci}}$ for $\lambda_{ce}/r = 250, 500,$ and 750 are 20.96, 10.3, and 6.8°, respectively. Below this threshold value of the incidence of the magnetic field, the collisional model is expected to apply. The potential drops in this low collisionality case have been calculated without assuming a source term in the fluid equation, neither in the continuity Eq. (12) nor in the conservation of the momentum Eqs. (9)–(11), as usually done in the literature in order to derive analytical expressions (see references by Ahedo[10] and Stangeby[15]). This is mainly possible because the Boltzmann relation holds for

electrons as long as $\theta > \theta*$ and $\theta > \theta_c$. In the high collisional regime, one has to consider a source term in order to solve the density profile in the quasi-neutral region.

2. $\lambda_{ci} \ll R$ or $\sin \theta < \frac{R}{\lambda_{ci}}$

In such a case, as explained previously, the Chodura sheath disappears, and the entire potential drop in the quasi-neutral region occurs between the sonic point defined by Eq. (17) and the center of the plasma, where it is assumed $V_x \simeq 0$. In order to evaluate this potential drop, we have to neglect the inertial terms in the set of Eqs. (9)–(11) for both ions and electrons and to assume a source term in the plasma. This procedure yields

$$V_{ix} = \frac{\mu_i}{C_i}E - \frac{D_i}{C_i}\frac{n'}{n},\qquad(25)$$

with

$$C_i = \frac{\nu_i^2 + \omega_{ci}^2}{\nu_i^2 + \omega_{ci}^2 \sin^2\theta}\qquad(26)$$

and ν_i and ω_{ci} the ion collision and cyclotron frequencies, respectively.

If $\theta \to \pi/2$, one recovers the classical result without the magnetic field effect with the mobility $\mu_i = \frac{|e|}{\nu_i M}$ and the diffusion coefficient $D_i = \frac{T_i}{\nu_i M}$. Applying the same reasoning to electrons, with their own coefficients C_e, μ_e, and D_e, assuming in the context of the plasma approximation that $V_{ix} \simeq V_{ex}$, it is possible to solve E as

$$E = \frac{D_i\frac{C_e}{C_i} - D_e}{\mu_i\frac{C_e}{C_i} + \mu_e}\frac{n'}{n}.\qquad(27)$$

Now, the conservation of the particle number is

$$\frac{\partial(nV_x)}{\partial x} = S.\qquad(28)$$

As explained previously, the ion number is kept constant during the simulations: each time one comes across the walls, a (ion, electron) couple is injected randomly in the plasma. During iteration time dt, in the steady state, there are $2\Gamma_w.A.dt$ ions reaching the walls, where A is the area of the studied plasma, Γ_w is the particle flux at a single wall, and factor 2 comes from the presence of 2 walls. The source term S in Eq. (28) can then be calculated, in $/m^3/s$ units, as $S = (2\Gamma_w A dt)/(ALdt) = 2\Gamma_w/L$.

Replacing Eq. (27) in (25) gives the particle flux $\Gamma(x) = nV_x(x)$

$$\Gamma = -\frac{D_e\mu_i + D_i\mu_e}{\mu_i C_e + \mu_e C_i}n' = -D_a^\theta n',\qquad(29)$$

with D_a^θ being the ambipolar diffusion coefficient which depends on the incidence of the magnetic field line with respect to the wall. Substituting in Eq. (28) yields

$$n''(x) = -\frac{2\Gamma_w}{LD_a^\theta}.\qquad(30)$$

The previous differential equation can be solved with the boundary conditions $n(L/2) \simeq n(-L/2) \simeq 0$, known as the

Schottky condition, and usually assumed in high collisional plasma.[31,32] This previous approximation leads to the resolution of the density profile in the quasi-neutral region, assuming that the sheath is very thin with respect to the latter, as

$$n(x) = \frac{\Gamma_w L}{4D_a^\theta}\left(1 - \frac{4x^2}{L^2}\right).\qquad(31)$$

In the steady state, we necessarily have $n(0) = n_0$ so that $\Gamma_w = \frac{4D_a^\theta n_0}{L}$. The quasi-neutral regions end at the sonic point S when the Debye sheath exists, otherwise at the walls if the quasi-neutrality does not break down within the plasma. Let us call V_{out} the velocity at the exit of the quasi-neutral region, such as $V_{out} = |\max(-C_s, V_x(-L/2))|$, assuming $V_x < 0$ at the vicinity of the left wall as depicted in Fig. 1. Then, when the plasma becomes supersonic before reaching the wall, $V_{out} = C_s$ (the velocity at the wall is necessarily $|V_x(-L/2)| > C_s$); else, $V_{out} = |V_x(-L/2)|$.

If we neglect the source term in the region separating the wall from the sonic point S, we can approximate $\Gamma_w = n_{out}V_{out}$, with n_{out} being the density at the considered point (sonic point S or the wall), which yields

$$\frac{n_{out}}{n_0} = \frac{4D_a^\theta}{LV_{out}}.\qquad(32)$$

Integrating Eq. (27) between the point (n_{out}, V_{out}) and the center of the plasma gives finally

$$\Delta\phi_{qn} = -\frac{D_iC_e - D_eC_i}{\mu_iC_e + \mu_eC_i}\ln\frac{4D_a^\theta}{L|V_{out}|}.\qquad(33)$$

Figure 7(b) shows the angular variation of the normalized velocity at the exit of the quasi-neutral region as explained above. For incidences larger than 15°, a space-charge field forms and the quasi-neutrality breaks down at the Bohm velocity. For grazing incidences, the exit velocity becomes $V_x(-L/2)$, which considerably decreases with θ for all mean-free-paths. In the same figure, we plot the modified Bohm velocity $C_{s\theta}$ [Eq. (17)], which is in a qualitative agreement with the simulations results. Other authors have derived a similar variation of the velocity as $C_{s\theta}$ at the exit of the plasma from fluid considerations or kinetic simulations.[15,16] In the following, we will then assume that $|V_{out}| = C_{s\theta}$ in the collisional model.

Figure 6(b) shows that in the high collisionality case ($\lambda_{ci} < R$), the collisional model [Eq. (33)] is in good agreement with the PIC simulation results, apart from the very grazing incidences, below 2°, where the calculated potential drop is twice that of the simulated one. In Fig. 5(b), it can be seen that the collisional model is also in good agreement with the simulated result in the lower collisionality case ($\lambda_{ci} > R$) for incidences smaller than 20°, i.e., smaller than θ_c. The model also reproduces very well the slope of $\Delta\phi_{qn}$ vs. θ for the range of mean-free-paths we investigated and can explain the change in polarity of the potential drop in the quasi-neutral region. However, just like in Fig. 6(b), the model gives a larger potential drop than the simulation results below 2° although the discrepancy is smaller than in Fig. 6(b).

In fact, for such a small incidence, the potential drop $\Delta\phi_{qn}$ is found to be opposite to the usual one, i.e., this is a regime where ions are pushed back into the plasma. The ambipolarity is maintained within the plasma, thanks to the ambipolar electric field, as shown in Fig. 3(b). However, at the proximity of the wall, over a distance, $\simeq r$, a small positive charge arises because electrons are still the fastest species in this non-collisional limited region of the plasma [see Fig. 3(a) for $\theta = 0.5^\circ$]. There is obviously a potential drop associated with this region scaling with r which we do not treat in a fluid model and which can explain the discrepancy observed for $\theta < 2^\circ$.

3. Ambipolar field transition

In the collisional pre-sheath, which separates the plasma from the Debye (point S) or the Chodura sheath (point C), particles are accelerated via an ambipolar field from a null velocity to the corresponding sonic point. Depending on the angle of incidence of the magnetic field and mean-free-path to Larmor radius ratios, the ambipolar field can be either negative and accelerate ions towards the wall or positive and push back ions into the plasma as seen in Fig. 3(b), for instance. The transition between both regimes can be evaluated by using Eq. (27). The sign of the ambipolar field changes when

$$D_i C_e = D_e C_i. \tag{34}$$

We assume for the sake of generality that $\lambda_{ci} = \gamma\lambda_{ce}$. For a given electron mean-free-path to Larmor radius ratio $\lambda_{ce}/r = \alpha$, we can derive from Eq. (34) a critical angle θ_p under which the ambipolar field is positive as

$$\sin^2\theta_p = \frac{1 - A + \alpha^2(\beta^2 - A)}{\alpha^2\left(A\beta^2 - 1 + \alpha^2\beta^2(A - 1)\right)}, \tag{35}$$

where $\beta^2 = \gamma^2\frac{T_e m}{T_i M}$ and $A^2 = \gamma^2\frac{T_i m}{T_e M}$. Note that this expression stands for any mean-free-path, for any collisional regime of both ions and electrons. Indeed, it is possible to assume that in the center of the plasma the velocity gradient is very small and that all left members of the set of Eqs. (9)–(11) can be neglected for each species.

Figure 7(c) shows a density plot, interpolated from our simulation results as explained previously, which depicts the normalized potential drop in the quasi-neutral region with respect to θ and the ratio λ_{ce}/r, the white contrast in the figure being associated with a null potential drop. For such a null $\Delta\phi_{qn}$, the ambipolar field is expected to change its direction. The critical angle $\theta_p = f(\lambda_{ce}/r)$ from Eq. (35) is also plotted in the figure, and it appears that it follows fairly well the white contrast of the density plot. This shows that the collisional model explains the transition in the ambipolarity, which is seen in Fig. 3(b). The critical angle is plotted in the same figure for $M/m = 1836$ (H$^+$), and it exhibits qualitatively a similar variation with λ_{ce}/r.

Note that this unexpected regime, where ions have to be slowed down with respect to electrons, appears at very grazing incidences or high collisionality; it does not coexist with a Debye sheath as shown in the density plot of Fig. 4(c). Moreover, as can be seen with the curve $\theta_p = f(\lambda_{ce}/r)$ in Fig. 7(c), there is a

threshold in the collisionality below which no critical angle θ_p can be found. It corresponds to the case where $\sin^2\theta_p < 0$ in Eq. (35). In this high collisional regime, ions are slowed down by the collisional drag, while electrons stay for a shorter time on a given field line because the ratio λ_{ce}/r decreases. Therefore, the potential drop in the plasma is, in this case, always positive with respect to the wall as seen in Fig. 2(e). This leads to the limit $\lambda_{ce}/r = 1$ where the system is completely demagnetized by collisions and where no magnetic effect delays the electron drift towards the wall.

IV. CONCLUSION

In this paper, we studied by means of PIC simulations the evolution of the potential drops in the different layers constituting the PWT, in the presence of a magnetic field tilted by θ with respect to the wall and of collisions with neutrals. We investigated a large range of collisionality for the ions, from $\lambda_{ci}/R = 0.11$ to 8.3, which was large enough to study the transition between two opposite regimes: one where the magnetic order was destroyed by collisions, to another one, where both ions and electrons were moving along the field line in the plasma. We showed that both the collisionality and the incidence of the magnetic field have important influences on the PWT characteristics, from the non-neutral Debye sheath to the quasi-neutral region.

We evidenced that in the high collisional regime, the Debye sheath disappears, the plasma being subsonic for any incidence, because the potential drop in the collisional pre-sheath is large enough to balance ions and electron losses at the walls. When the ion mean-free-path increases and collisions with neutrals become less and less frequent, the potential drop in the Debye sheath increases because a space-charge field is needed to accelerate ions and slow down electrons. However, when the incidence decreases, ion mobility towards the wall increases with respect to electrons due to collisions. That is why the potential drop in the Debye sheath decreases with θ, which is expected in the collisionless limit because of the particle flux reduction at the wall; here, the effect is exacerbated by collisions.

Concerning the quasi-neutral region, we evidence two trends: when the ion mean-free-path is very large with respect to the ion Larmor radius ($\lambda_{ci} \gg R$), the plasma flows parallel to the magnetic field line in the pre-sheath, which scales with λ_{ci}, until it enters the Chodura region. At the exit of the Chodura sheath, the quasi-neutrality breaks down, and the total potential drop between the Debye sheath entrance and the center of the plasma follows the variation $e\Delta\phi_{qn}/T_e = \ln(\sin\theta) - 0.5$. When the angle of incidence of the magnetic field is such as $\theta \leq \theta_c = \arcsin R/\lambda_{ci}$, and although the ion mean-free-path is quite larger than the Larmor radius, the Chodura sheath disappears and merges with the collisional pre-sheath. For such incidences, the potential drop in the quasi-neutral region follows a collisional law, where the inertia of both ions and electrons is neglected. The same collisional law successfully models $\Delta\phi_{qn}$ when $\lambda_{ci} < R$, in the regime of high collisionality of the ions.

It is important to notice that in our fluid model, we have neglected the momentum loss due to ionization in the set of fluid Eqs. (9) and (10). Yet, the random injection model, which is used in the PIC simulations to conserve the total number of ions, induces a drag because each particle injected from the nominal Maxwellian distribution has to be accelerated to the average fluid velocity; therefore, the injection model may influence the potential drops determined in our numerical study in every part of the PWT, even in the Debye sheath.

In a plasma reactor such as ALINE,[33] with an hydrogen plasma such as $T_e = T_i = 2$ eV and B = 0.1 T, and an expected elastic collisional frequency for electrons with neutrals of the order of $\nu_e = 45$ MHz, we have $\lambda_{ce}/r = 276$ or $\lambda_{ci}/R = 1.6$, assuming $\lambda_{ce} = 4 \times \lambda_{ci}$. In the conditions met in the scrape-off layers (SOL) of tokamaks,[14,34] with $T_e = 20$ eV and B = 2 T, we have $\lambda_{ce}/r = 5525$ or $\lambda_{ci}/R = 32$ for hydrogen. The critical angle θ_c below which collisions make the Chodura sheath disappear and merge with the collisional pre-sheath is of the order of $38°$ for ALINE and $1.78°$ for the SOL of tokamaks. This is quite larger and of the same order of magnitude than $\theta^* = 4.74°$, the theoretical angle at which the Debye sheath is expected to vanish in the collisionless limit. Moreover, the critical angle θ_p below which the potential drop in the pre-sheath is expected to reverse, and push-back ions into the plasma, is of $\theta_p = 2.31°$ for a reactor such as ALINE and of $0.136°$ for the SOL of tokamaks. Collisions with neutrals, and other phenomena inducing a similar drift of the particles perpendicularly to the field line (turbulence, anomalous transport, electron-ion collisions, shear velocity...), may then affect significantly the potential drops in the PWT, in both the Debye sheath and the quasi-neutral region, for relatively large angles, in plasma reactors with the characteristics of ALINE. The effect would be more subtle for warmer and strongly magnetized plasmas.

ACKNOWLEDGMENTS

REFERENCES

[1] P. Chabert and N. Braithwaite, *Physics of Radio-frequency Plasmas* (Cambridge University Press, 2011), pp. 1–17.

[2] R. A. Pitts, J. P. Coad, D. P. Coster, G. Federici, W. Fundamenski, J. Horacek, K. Krieger, A. Kukushkin, J. Likonen, G. F. Matthews, M. Rubel, and J. D. Strachan, Plasma Phys. Controlled Fusion **47**, B303 (2005).

[3] H. B. Garett, Rev. Geophys. **19**, 577, https://doi.org/10.1029/RG019i004p00577 (1981).

[4] D. Bohm, in *The Characteristics of Electrical Discharges in Magnetic Fields*, edited by A. Guthrie and R. K. Wakerling (McGraw-Hill, New York, 1949), p. 77.

[5] K. U. Riemann, J. Phys. D: Appl. Phys. **24**, 493 (1991).

[6] D. D. Tskhakaya, B. Eliasson, P. K. Shukla, and S. Kuhn, Phys. Plasma **11**, 3945 (2004).

[7] K.-B. Persson, Phys. Fluids **5**, 1625 (1962).

[8] R. Chodura, Phys. Fluids **25**, 1628 (1982).

[9] P. Stangeby, Phys. Plasmas **2**, 702 (1995).

[10] E. Ahedo, Phys. Plasma **4**, 4419 (1997).

[11] K. U. Riemann, Phys. Plasma **1**, 552 (1994).

[12] S. Devaux and G. Manfredi, Phys. Plasma **13**, 083504 (2006).

[13] D. D. Tskhakaya and L. Kos, Phys. Plasma **21**, 102115 (2014).

[14] P. Stangeby, C. Pitcher, and J. Elder, Nucl. Fusion **32**, 2079 (1992).

[15] P. Stangeby, Nucl. Fusion **52**, 083012 (2012).

[16] D. Coulette and G. Manfredi, Plasma Phys. Controlled Fusion **58**, 025008 (2016).

[17] D. D. Tskhakaya, P. K. Shukla, B. Eliasson, and S. Kuhn, Phys. Plasma **12**, 103503 (2005).

[18] N. S. Krasheninnikova, X. Tang, and V. S. Roytershteyn, Phys. Plasma **17**, 057103 (2010).

[19] K. Theilhaber and C. K. Birdsall, Phys. Fluids B **1**, 2244 (1989).

[20] K. Theilhaber and C. K. Birdsall, Phys. Fluids B **1**, 2260 (1989).

[21] M. J. Gerver, S. E. Parker, and K. Theilhaber, Phys. Fluids B **2**, 1069 (1990).

[22] D. L. Holland, B. D. Fried, and G. J. Morales, Phys. Fluids B **5**, 1723 (1993).

[23] U. Daybelge and B. Bein, Phys. Fluids **24**, 1190 (1981).

[24] J. Moritz, E. Faudot, S. Devaux, and S. Heuraux, Phys. Plasmas **23**, 062509 (2016).

[25] J. Moritz, E. Faudot, S. Devaux, and S. Heuraux, Phys. Plasmas **25**, 013534 (2018).

[26] M. Lieberman and A. Lichtenberg, *Principles of Plasma Discharges and Material Processing* (Wiley-Interscience, 2005), p. 8.

[27] F. Taccogna, R. Schneider, K. Matyash, S. Longo, M. Capitelli, and D. Tskhakaya, J. Nucl. Mater. **363**, 437 (2007).

[28] R. Bisswell, P. Johnson, and P. Stangeby, Phys. Fluid B **1**, 1133 (1989).

[29] P. C. Stangeby, *The Plasma Boundary of Magnetic Fusion Devices* (Institute of Physics Publishing, London, 2000), p. 413.

[30] D. Tskhakaya and S. Kuhn, J. Nucl. Mater. **313**, 1119 (2003).

[31] P. Chabert and N. Braithwaite, *Physics of Radio-frequency Plasmas* (Cambridge University Press, 2011), p. 86.

[32] W. Schottky, Phys. Z. **25**, 635 (1924).

[33] E. Faudot, S. Devaux, J. Moritz, S. Heuraux, P. M. Cabrera, and F. Brochard, Rev. Sci. Instrum. **86**, 063502 (2015).

[34] J. Bak, R. Pitts, H. Kim, H. Lee, C. Bin, J. Juhn, S. Hong, O. Garcia, R. Kube, and D. C. Seo, Nucl. Mater. Energy **12**, 1270 (2017).